Fractional Fourier transform in temporal ghost imaging with classical light

Tero Setälä,[1] Tomohiro Shirai,[2] and Ari T. Friberg[1,3,*]

[1]*Department of Applied Physics, Aalto University, P.O. Box 13500, FI-00076 Aalto, Finland*

[2]*Photonics Research Institute, National Institute of Advanced Industrial Science and Technology, 1-2-1 Namiki, Tsukuba 305-8564, Japan*

[3]*Department of Physics and Mathematics, University of Eastern Finland, P.O. Box 111, FI-80101 Joensuu, Finland*

(Received 5 July 2010; published 12 October 2010)

We investigate temporal, second-order classical ghost imaging with long, incoherent, scalar plane-wave pulses. We prove that in rather general conditions, the intensity correlation function at the output of the setup is given by the fractional Fourier transform of the temporal object. In special cases, the correlation function is shown to reduce to the ordinary Fourier transform and the temporal image of the object. Effects influencing the visibility and the resolution are considered. This work extends certain known results on spatial ghost imaging into the time domain and could find applications in temporal tomography of pulses.

DOI: 10.1103/PhysRevA.82.043813 PACS number(s): 42.25.Kb, 42.30.Va, 42.30.Kq

I. INTRODUCTION

Correlation imaging is a method to acquire an image of the object by measuring an intensity correlation function instead of the intensity distribution [1]. The second-order imaging is based on transmitting mutually correlated light beams through two arms: a test arm containing an object and a reference arm that includes an imaging system (e.g., a lens). The intensity distribution in the reference arm is scanned, whereas the total intensity in the test arm is detected. By correlating the intensities in the outputs of the two arms, spatial (image) or spectral (Fourier transform, FT) information of the object is obtained depending on the choice of the parameters. This kind of correlation imaging is often referred to as ghost imaging since the arm in which the intensity distribution is scanned does not contain the object.

Ghost imaging has its roots in quantum-mechanical entanglement and it was first demonstrated [2,3] for two-photon light (biphotons) generated in spontaneous parametric down-conversion [4]. A few years later, it was observed that ghost imaging does not necessitate nonlocal correlations of entangled photons but can be realized with classical, mutually correlated light beams [5]. In particular, classical, pseudothermal light with a random speckle structure enables ghost imaging without any reference to quantum effects [6–8]. Most works on ghost imaging, both classical and quantum, have concentrated on acquiring spatial information on the object, i.e., its image or far-field (spatial-frequency) distribution. However, it was recently pointed out that the two-photon coincidence detection amplitude obeys equations of motion similar to those that the correlations of classical, partially coherent plane-wave pulses do in linearly dispersive media [9,10]. This observation suggests that certain quantum-mechanical, time-domain entanglement phenomena, e.g., nonlocal temporal and spectral pulse shaping [11,12], could be mimicked by classical partially coherent light.

In this work, we consider temporal ghost imaging with long, classical plane-wave pulses having a short coherence time. We show that the correlation between the intensity fluctuations at the ends of the two arms of the ghost-imaging scheme is given by a fractional Fourier transform (FrFT) of the temporal object in the test arm. As an imaging element we employ a temporal lens [13] in the reference arm. Choosing the dispersion properties of the arms and the "focal length" of the lens suitably, the general result can be reduced to an ordinary Fourier transform as well as to an image of the object, providing spectral and temporal information on the object, respectively. Somewhat analogous works dealing with spatial-domain ghost imaging have been reported previously [14,15]. Entangled-photon Fourier optics has also been considered earlier [16]. Time-domain ghost imaging is applicable in nonlocal temporal sensing and imaging. Furthermore, in analogy with its spatial counterpart [17], the time-domain fractional Fourier transform can be useful in a variety of applications in temporal optics and processing of time-dependent signals.

This paper is organized as follows. In Sec. II we describe the temporal ghost-imaging setup and discuss its properties, such as visibility and resolution. In Sec. III we show that the intensity correlation function is generally given by a fractional Fourier transform of the object, which in special cases reduces to an ordinary Fourier transform and an image. Finally, in Sec. IV, we briefly summarize the work. Certain mathematical details are presented in Appendixes A and B.

II. TEMPORAL SECOND-ORDER GHOST-IMAGING SETUP

A long, temporally incoherent, scalar plane-wave pulse whose two-time coherence function is to a good approximation given by

$$\Gamma_0(t_1',t_2') = I_0\delta(t_2' - t_1'), \tag{1}$$

where I_0 is the intensity, is split into two arms of an interferometer as shown in Fig. 1. The pulse can be generated, e.g., by amplified spontaneous emission or supercontinuum radiation. The upper arm, called the reference arm, consists of a temporal lens having a transmission function $\exp(it^2/2\gamma)$, γ being a real quantity ("focal length"), and two sections of optical single-mode fiber characterized by the group-delay dispersion (GDD) parameters Φ_a and Φ_b. The quadratic phase modulation of the

*Also at the Department of Microelectronics and Applied Physics, Royal Institute of Technology (KTH), Electrum 229, SE-164 40 Kista, Sweden.

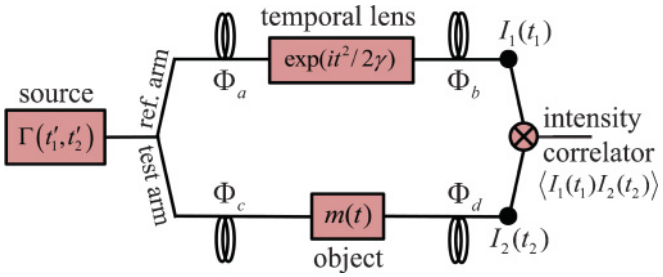

FIG. 1. (Color online) Illustration of the geometry for temporal ghost imaging. Light from a source is split into two mutually correlated beams which are directed to the reference and test arms. The reference arm contains two sections of single-mode fiber and a temporal lens characterized by the "focal length" γ. The test arm likewise contains two fiber sections and an object $m(t)$ between them. The fibers are characterized by the group-delay dispersion parameters Φ_i, with $i = (a,b,c,d)$. The output intensities of the arms, $I_i(t_i)$, with $i = (1,2)$, are measured and correlated.

temporal lens is a time-domain analog to the phase change due to a conventional lens. In practice, the temporal lens can be implemented with electro-optic phase modulators or by other nonlinear phenomena [13,18,19]. The lower arm, the test arm, contains a temporal object with a deterministic variation $m(t)$, and two sections of single-mode fiber with dispersion parameters Φ_c and Φ_d. The GDD parameters of the fibers are of the form $\Phi_i = \beta_{2i} z_i$, $i = (a,b,c,d)$, where β_{2i} is the group-velocity dispersion (GVD) coefficient, which may be positive or negative, and z_i denotes the length of fiber. The evolution of plane-wave pulses in first-order dispersive fibers is governed, by the space-time duality [20,21], with an equation analogous to the one-dimensional paraxial diffraction formula. The instantaneous intensities, $I_i(t_i)$, $i = (1,2)$, at the outputs of the arms are then recorded as a function of time, and their correlation function is computed. The role of the detector speed is discussed below.

The slowly-varying envelopes of a realization of the random optical fields at the output of the arms, $E_i(t)$, can be written as

$$E_i(t) = \int_{-\infty}^{\infty} E_0(t') K_i(t,t')\, dt', \quad i = (1,2), \tag{2}$$

where $E_0(t)$ is the input realization, and $i = (1,2)$ refer to the reference arm and the test arm, respectively. Both arms consist of a cascade of linear elements whose effect on the field is contained in the kernels $K_{1,2}(t,t')$. For the reference arm the kernel is of the form [10,21],

$$K_1(t,t') = \frac{1}{2\pi}\sqrt{\frac{i}{\Phi_a}}\sqrt{\frac{i}{\Phi_b}}\int_{-\infty}^{\infty} \exp\left(\frac{it''^2}{2\gamma}\right) \times \exp\left[-i\frac{(t''-t')^2}{2\Phi_a} - i\frac{(t''-t)^2}{2\Phi_b}\right] dt'', \tag{3}$$

whereas for the test arm we have

$$K_2(t,t') = \frac{1}{2\pi}\sqrt{\frac{i}{\Phi_c}}\sqrt{\frac{i}{\Phi_d}}\int_{-\infty}^{\infty} m(t'') \times \exp\left[-i\frac{(t''-t')^2}{2\Phi_c} - i\frac{(t''-t)^2}{2\Phi_d}\right] dt''. \tag{4}$$

Equations (2)–(4) hold for narrow-band light for which a fiber effectively acts as a Gaussian chirp filter; integrations with respect to time can be taken to infinity without violating causality [21]. These equations determine the instantaneous intensities at the outputs, explicitly given by $I_i(t) = |E_i(t)|^2$, with $i = (1,2)$. Detectors are not infinitely fast, rather they integrate over a period of time. Thus, the quantities $I_i(t)$, in practice, are short-time averages of the instantaneous intensities accounting for the detectors' speed and spectral response. This will influence the resolution and visibility of the imaging scheme. Temporal resolutions on the order of 100 ps are obtainable with present detectors [22]. However, detection schemes based on two-photon absorption and capable of femtosecond resolution are emerging [23], paving the way toward nearly time-resolved intensity correlation measurements.

The intensity correlation function of the output fields in the two arms, then, is

$$\begin{aligned} G^{(2)}(t_1,t_2) &= \langle I_1(t_1) I_2(t_2)\rangle \\ &= \int_{-\infty}^{\infty}\int_{-\infty}^{\infty}\int_{-\infty}^{\infty}\int_{-\infty}^{\infty} \langle E_0^*(t_1') E_0^*(t_2') E_0(t_1'') E_0(t_2'')\rangle \\ &\quad \times K_1^*(t_1,t_1') K_2^*(t_2,t_2') K_1(t_1,t_1'') \\ &\quad \times K_2(t_2,t_2'') dt_1' dt_2' dt_1'' dt_2'', \end{aligned} \tag{5}$$

where the angle brackets denote ensemble averaging. For sufficiently chaotic fields obeying Gaussian statistics the fourth-order correlation function present in the integrand can be expressed in terms of the second-order functions by using the moment theorem [24]. In doing so, Eq. (5) takes on the form,

$$G^{(2)}(t_1,t_2) = \langle I_1(t_1)\rangle\langle I_2(t_2)\rangle + |\Gamma(t_1,t_2)|^2, \tag{6}$$

where

$$\Gamma(t_1,t_2) = \int_{-\infty}^{\infty}\int_{-\infty}^{\infty} \Gamma_0(t_1',t_2') K_1^*(t_1,t_1') K_2(t_2,t_2')\, dt_1' dt_2'. \tag{7}$$

In this equation $\Gamma_0(t_1',t_2')$ is the two-time coherence function of the incident field, given by Eq. (1), which when substituted into Eq. (7), leads to

$$\Gamma(t_1,t_2) = I_0 \int_{-\infty}^{\infty} K_1^*(t_1,t_1') K_2(t_2,t_1')\, dt_1'. \tag{8}$$

The quantity $|\Gamma(t_1,t_2)|^2$ is analogous to the two-photon coincidence probability in quantum-mechanical ghost imaging, and it contains, in a form of temporal correlation, information on the object $m(t)$. Introducing the intensity fluctuation as $\Delta I(t) = I(t) - \langle I(t)\rangle$, it is readily shown that

$$\langle \Delta I_1(t_1) \Delta I_2(t_2)\rangle = |\Gamma(t_1,t_2)|^2, \tag{9}$$

indicating that the function $|\Gamma(t_1,t_2)|^2$ can classically be interpreted as a measure of the strength of the correlation between the intensity fluctuations at the outputs of the two arms.

The averaged intensities in Eq. (6) constitute a background term that reduces the visibility in ghost imaging with classical light. The visibility can be defined by [25]

$$\mathcal{V} = \frac{g^{(2)}_{\max}(t_1,t_2) - g^{(2)}_{\min}(t_1,t_2)}{g^{(2)}_{\max}(t_1,t_2) + g^{(2)}_{\min}(t_1,t_2)}, \tag{10}$$

where

$$g^{(2)}(t_1,t_2) = \frac{G^{(2)}(t_1,t_2)}{\langle I_1(t_1)\rangle\langle I_2(t_2)\rangle}, \tag{11}$$

and $g^{(2)}_{\max,\min}$ denote nearby maxima and minima. It can be shown that $1 \leqslant g^{(2)}(t_1,t_2) \leqslant 2$, and, therefore, the visibility in second-order classical ghost imaging with light obeying Gaussian statistics is limited to $\mathcal{V}_{\max} = 1/3$. The finite detector response time will further reduce the visibility as it smoothens the function $G^{(2)}(t_1,t_2)$. However, in second-order and especially in higher-order classical ghost imaging with Gaussian light the visibility can be significantly better, and even 1 as in quantum imaging, provided the background intensities can be subtracted optically or electronically [25,26]. In practice, an important parameter characterizing the image quality is the signal-to-noise ratio (SNR) which recently has received much attention in ghost imaging [27]. It has been shown that SNR can be improved by novel techniques such as compressive ghost imaging [28] and, in particular, differential ghost imaging [29], which could be applied also in the context of temporal ghost imaging. The resolution, on the other hand, is determined by the detector speed and the coherence time of light. In this work the incident light is taken temporally fully incoherent with zero coherence time, implying the best obtainable resolution.

III. FRACTIONAL FOURIER TRANSFORMATION OF THE OBJECT IN THE INTENSITY CORRELATION FUNCTION

Inserting Eqs. (3) and (4) into Eq. (8) leads, after some straightforward developments outlined in Appendix A, to

$$\begin{aligned}\Gamma(t_1,t_2) = I_0\sqrt{\frac{\gamma}{2\pi r\Phi_d}}\sqrt{\frac{1}{1-i\cot\alpha}}\exp\left[i(\psi-\pi/2)\right]\\ \times \exp\left(-\frac{i}{2\Phi_d}t_2^2\right)\exp\left[\frac{i}{2r}(\Phi_a-\Phi_c-\gamma)t_1^2\right]\\ \times \exp\left(-i\omega^2\cot\alpha/2\right)\mathcal{M}_\alpha(\omega),\end{aligned} \tag{12}$$

where

$$r = (\Phi_a-\Phi_c)(\Phi_b-\gamma) - \Phi_b\gamma. \tag{13}$$

The parameter ψ is a constant, time-independent phase specified by the dispersion parameters and the focal length. Its explicit form is not relevant for this work. In particular,

$$\begin{aligned}\mathcal{M}_\alpha(\omega) = \sqrt{\frac{1-i\cot\alpha}{2\pi}}\exp(i\omega^2\cot\alpha/2)\int_{-\infty}^{\infty} m(t)\\ \times \exp[-i\omega t\csc\alpha + it^2\cot\alpha/2]\,dt,\end{aligned} \tag{14}$$

is the fractional Fourier transform of order α [17,30] of the object $m(t)$. In Eqs. (12) and (14), the quantities α and ω are determined by the GDD parameters of the fiber sections, γ of the temporal lens, and times t_1 and t_2 as follows:

$$\cot\alpha = \frac{\Phi_b}{r} - \frac{1}{\Phi_d} - \frac{\gamma}{r}, \tag{15}$$

$$\omega\csc\alpha = -\frac{t_2}{\Phi_d} - \frac{\gamma t_1}{r}. \tag{16}$$

According to Eq. (12), the modulation in Eq. (6) assumes the form,

$$|\Gamma(t_1,t_2)|^2 = \frac{I_0^2}{2\pi}\left|\frac{\gamma\sin\alpha}{r\Phi_d}\right||\mathcal{M}_\alpha(\omega)|^2. \tag{17}$$

Thus, the temporal modulation of the intensity correlation function in second-order classical ghost imaging is, in the general conditions assumed in this work, determined by the fractional Fourier transform of the object in the test arm. In special cases, the general result reduces to the ordinary Fourier transform and the temporal image of the object, as will be shown in subsequent sections.

The quantity $g^{(2)}(t_1,t_2)$ in Eq. (11) that specifies the visibility contains $\langle I_1(t_1)\rangle$ and $\langle I_2(t_2)\rangle$ in the denominator. For (infinitely) long δ-correlated pulses as in Eq. (1) one finds that $\langle I_1(t_1)\rangle = \infty$, while $\langle I_2(t_2)\rangle$ remains finite provided the modulation $m(t)$ is of limited duration. Hence, the use of a Dirac δ function leads to zero visibility due to the divergence of $\langle I_1(t_1)\rangle$. However, this is an unphysical result since the correlation function has to remain finite. A more accurate analysis implies that $\langle I_1(t_1)\rangle = I_0|\gamma/(\gamma-\Phi_b)|\mu(0)$, where $\mu(\tau)$ is the normalized temporal correlation function of the input light, i.e., $\Gamma_0(\tau) = I_0\mu(\tau)$ with $\mu(0) = 1$. This corresponds to a nonzero visibility. The visibility can also be enhanced by using shorter (finite) pulses [31]. For example, assuming that the input field $E_0(t)$ in Eq. (2) is δ correlated but nonzero only within a finite interval $-T \leqslant t \leqslant T$ leads to $\langle I_1(t_1)\rangle = I_0T|\gamma|/\pi|\gamma(\Phi_a+\Phi_b) - \Phi_a\Phi_b|$. As mentioned before, the visibility can be improved within the limits of noise by measuring $\langle I_1(t_1)\rangle$ and $\langle I_2(t_2)\rangle$ and subtracting their product from the intensity-correlation signal. By removing the background completely, the visibility in classical ghost imaging can reach the maximum value of 1.

A. Reduction to Fourier transform

The fractional Fourier transform given in Eq. (14) reduces to the ordinary Fourier transform when $\alpha = \pi/2$ [17]. According to Eq. (15), this case is encountered when the system parameters are chosen such that

$$\frac{\Phi_b}{r} - \frac{1}{\Phi_d} - \frac{\gamma}{r} = 0. \tag{18}$$

The quantity ω then is given by Eq. (16) as

$$\omega = -\frac{t_2}{\Phi_d} - \frac{\gamma t_1}{r}, \tag{19}$$

and the function $\Gamma(t_1,t_2)$ assumes the form,

$$|\Gamma(t_1,t_2)|^2 = \frac{I_0^2}{2\pi}\left|\frac{\gamma}{r\Phi_d}\right|\left|M\left(-\frac{t_2}{\Phi_d} - \frac{\gamma t_1}{r}\right)\right|^2. \tag{20}$$

In the previous equation the function $M(\omega)$ is the Fourier transform of $m(t)$, defined as

$$M(\omega) = \frac{1}{\sqrt{2\pi}} \int_{-\infty}^{\infty} m(t) \exp(-i\omega t)\, dt. \tag{21}$$

We note that the case $\alpha = -\pi/2$ would correspond to an inverse Fourier transform.

Equation (18) indicates that there exist several possibilities to obtain a Fourier transform of the object in the intensity correlation function. For example, by choosing $\Phi_a = \Phi_c$ for the dispersion parameters, and $1/\gamma = 1/\Phi_b - 1/\Phi_d$ for the temporal lens, we find that

$$|\Gamma(t_1,t_2)|^2 = \frac{I_0^2}{2\pi} \left| \frac{1}{\Phi_b \Phi_d} \right| \left| M\left(\frac{t_1}{\Phi_b} - \frac{t_2}{\Phi_d} \right) \right|^2. \tag{22}$$

On the other hand, if $\Phi_a = \Phi_d$ and $1/\gamma = 1/\Phi_b - 1/\Phi_c$, then

$$|\Gamma(t_1,t_2)|^2 = \frac{I_0^2}{2\pi} \left| \frac{\Phi_c}{\Phi_b \Phi_d^2} \right| \left| M\left(\frac{\Phi_c t_1}{\Phi_b \Phi_d} - \frac{t_2}{\Phi_d} \right) \right|^2. \tag{23}$$

In particular, for arbitrary GDD parameters, choosing the "focal length" of the temporal lens as

$$\gamma = \frac{\Phi_b(\Phi_a - \Phi_c - \Phi_d)}{\Phi_a + \Phi_b - \Phi_c - \Phi_d}, \tag{24}$$

results in the Fourier transform,

$$|\Gamma(t_1,t_2)|^2 = \frac{I_0^2}{2\pi} \left| \frac{\Phi_a - \Phi_c - \Phi_d}{\Phi_b \Phi_d^2} \right| \times \left| M\left[-\frac{(\Phi_a - \Phi_c - \Phi_d) t_1}{\Phi_b \Phi_d} - \frac{t_2}{\Phi_d} \right] \right|^2. \tag{25}$$

We emphasize that the previous results pertaining to the Fourier transform of a temporal object are analogous to the existence of a Fourier plane in a spatial-lens imaging system. Adjustment of the GDD parameters and γ in the temporal imaging setup corresponds to altering the object position, focal length of the lens, and the position of the associated Fourier plane (location of the source) in the spatial imaging system [32].

Earlier, a Fourier transform of the object was found in a lensless ghost-imaging scheme [10]. In our formalism that geometry corresponds to the case $\Phi_a + \Phi_b = \Phi_c + \Phi_d$, for which Eq. (24) implies that $\gamma = \infty$ as expected for a lensless setup. With these parameters Eq. (25) turns into

$$|\Gamma(t_1,t_2)|^2 = \frac{I_0^2}{2\pi} \left| \frac{1}{\Phi_d^2} \right| \left| M\left(\frac{t_1 - t_2}{\Phi_d} \right) \right|^2, \tag{26}$$

which is Eq. (11) in Ref. [10]. This result obtained for the lensless geometry corresponds to the Fraunhoffer diffraction pattern in the spatial domain, and could be called temporal ghost diffraction.

B. Reduction to image

If $\alpha = \pi$ then $\cot\alpha$ and $\csc\alpha$ in Eqs. (15) and (16), respectively, diverge. In this case Eq. (14) could be evaluated with appropriate limiting procedures [17]. Alternatively, we first note that Eq. (15) necessarily implies $r = 0$, which with the help of Eq. (13) leads to the temporal analog of the thin-lens equation in spatial ghost imaging [33], viz.,

$$\frac{1}{\gamma} = \frac{1}{\Phi_b} + \frac{1}{\Phi_a - \Phi_c}. \tag{27}$$

When the previous condition holds, the function $\Gamma(t_1,t_2)$ takes on the form (see Appendix B),

$$\Gamma(t_1,t_2) = \frac{I_0}{\sqrt{-2\pi i s \Phi_d}} \exp(i\psi') m\left(\frac{t_1}{s} \right) \times \exp\left[-\frac{i}{2\Phi_d} \left(\frac{t_1}{s} - t_2 \right)^2 \right] \times \exp\left[\frac{i}{2\Phi_b} \left(1 - \frac{1}{s} \right) t_1^2 \right], \tag{28}$$

where ψ' is a time-independent phase term, and

$$s = \frac{\Phi_b}{\Phi_c - \Phi_a}. \tag{29}$$

The absolute value squared of Eq. (28) is

$$|\Gamma(t_1,t_2)|^2 = \frac{I_0^2}{2\pi} \left| \frac{1}{\Phi_d s} \right| \left| m\left(\frac{t_1}{s} \right) \right|^2, \tag{30}$$

indicating that an image of the object is contained in the intensity correlation function.

The formation of the image in classical spatial correlation imaging with pseudothermal light can be explained in terms of the intensity-weighted speckle patters [34]. In the time domain, an analogous interpretation holds but the speckle patterns are replaced by the random intensities of the field realizations, whose weighted average produces the image. The weighting is determined by the overlap of the temporal object and the intensity. The higher the intensity of a realization during the modulation $m(t)$, the larger the weighting for that particular realization.

We see from Eq. (30) that the quantity $|s|$ acts as a magnification factor for the image. For $|s| > 1$ the image is magnified in time, whereas for $|s| < 1$ it is demagnified. These cases, respectively, correspond to $m(t/s)$ being longer or shorter than $m(t)$. In addition, s can be either positive or negative leading to an erect or an inverted image. When the image is inverted in time, the back tail of the object $m(t)$ turns into the front end in the image. If the lens is removed (i.e., $\gamma \to \infty$), then $s = 1$ and the output is a nonmagnified image of the object. Equation (30) also shows that the image is independent of time t_2. Therefore, in measuring $|\Gamma(t_1,t_2)|^2$ the intensity $I_1(t_1)$ in the reference arm is scanned as a function of t_1, such that the interval of t_1 covers and is longer than the scaled temporal image of $m(t)$. This intensity is correlated with $I_2(t_2)$ of the test arm where the interval of t_2 is not required to overlap with $m(t)$, but can be arbitrary. Note also that (with time-resolved detection) the image resolution is infinitely accurate, consistently with the fact that the source is temporally fully incoherent. Furthermore,

Eq. (30) suggests that information on a pure phase object is not obtained by the ghost-imaging setup considered in this work.

IV. SUMMARY

It is a known fact that the optical field at any plane behind the lens in a spatial imaging system is given by a fractional Fourier transform of the object in front of the lens. In this work we have demonstrated that an analogous result holds in temporal, classical ghost imaging with long, incoherent plane-wave pulses. The coherence time of the source and the detector response time influence the resolution and visibility of the resulting signal. We also showed that by adjusting the temporal lens and the dispersion properties of the single-mode fibers constituting the setup, the correlation between the intensity fluctuations at the output can be reduced to an image and an ordinary Fourier transform of the object. These cases correspond to the existence of the image plane and the Fourier plane in a conventional spatial imaging system. An important application of our results deals with time-domain tomography of pulsed fields. The fractional Fourier transforms correspond to projections of the time-frequency Wigner function from which the pulse shape can be determined [35].

ACKNOWLEDGMENTS

Useful discussions with Henri Kellock are acknowledged. This research was funded by the Academy of Finland (Grants No. 128331 and No. 13135030). Part of the work was done when T. Shirai was visiting the optics and photonics group at Aalto University.

APPENDIX A: DERIVATION OF EQ. (12)

Substituting Eqs. (3) and (4) into Eq. (8) leads to

$$\begin{aligned}\Gamma(t_1,t_2) = {} & \frac{(2\pi)^{-3/2} I_0}{\sqrt{i\Phi_b\Phi_d(\Phi_a-\Phi_c)}} \exp(i\psi') \\ & \times \int_{-\infty}^{\infty} m(t') \exp\left[-\frac{i}{2\Phi_d}(t'-t_2)^2\right] \\ & \times \int_{-\infty}^{\infty} \exp\left(-\frac{it''^2}{2\gamma}\right) \exp\left[\frac{i}{2\Phi_b}(t''-t_1)^2\right] \\ & \times \exp\left[\frac{i(t''-t')^2}{2(\Phi_a-\Phi_c)}\right] dt''dt', \end{aligned} \tag{A1}$$

where ψ' is a constant (time-independent) phase term determined by the geometry, and we have employed the equation,

$$\begin{aligned}&\int_{-\infty}^{\infty} \exp\left[\frac{i}{2u}(t''-\tau)^2\right] \exp\left[-\frac{i}{2v}(t'-\tau)^2\right] d\tau \\ &= \sqrt{\frac{2\pi uv}{i\,(u-v)}} \exp\left[\frac{i(t''-t')^2}{2(u-v)}\right]. \end{aligned} \tag{A2}$$

Integration with respect to t'' in Eq. (A1) can be carried out and is

$$\begin{aligned}&\int_{-\infty}^{\infty} \exp\left[-\frac{it''^2}{2\gamma} + \frac{i}{2\Phi_b}(t''-t_1)^2 + \frac{i(t''-t')^2}{2(\Phi_a-\Phi_c)}\right] dt'' \\ &= (-1)^{1/4}\sqrt{\frac{2\pi\gamma\Phi_b(\Phi_c-\Phi_a)}{r}} \\ &\quad \times \exp\left\{\frac{i}{2r}\left[(\Phi_a-\Phi_c)t_1^2 - \gamma(t_1-t')^2 + \Phi_b t'^2\right]\right\}, \end{aligned} \tag{A3}$$

where r is defined in Eq. (13). Using the previous formula in Eq. (A1) results in

$$\begin{aligned}\Gamma(t_1,t_2) = {} & \frac{I_0}{2\pi i}\sqrt{\frac{\gamma}{r\Phi_d}} \exp(i\psi) \int_{-\infty}^{\infty} m(t') \\ & \times \exp\left[-\frac{i}{2\Phi_d}(t'-t_2)^2\right] \exp\left\{\frac{i}{2r}\left[(\Phi_a-\Phi_c)t_1^2\right.\right. \\ & \left.\left. - \gamma(t_1-t')^2 + \Phi_b t'^2\right]\right\} dt', \end{aligned} \tag{A4}$$

where ψ is a constant geometry-dependent phase, in general, $\psi \neq \psi'$. The previous expression, in turn, can be arranged as follows:

$$\begin{aligned}\Gamma(t_1,t_2) = {} & \frac{I_0}{2\pi i}\sqrt{\frac{\gamma}{r\Phi_d}} \exp(i\psi) \exp\left(-\frac{i}{2\Phi_d}t_2^2\right) \\ & \times \exp\left[\frac{i}{2r}(\Phi_a-\Phi_c-\gamma)\,t_1^2\right] \\ & \times \int_{-\infty}^{\infty} m(t') \exp\left[\frac{i}{2}\left(\frac{\Phi_b}{r} - \frac{1}{\Phi_d} - \frac{\gamma}{r}\right)t'^2\right] \\ & \times \exp\left[i\left(\frac{t_2}{\Phi_d} + \frac{\gamma t_1}{r}\right)t'\right] dt'. \end{aligned} \tag{A5}$$

Introducing next the parameters given in Eqs. (15) and (16), Eq. (A5) can be written in the form of Eq. (12).

APPENDIX B: DERIVATION OF EQ. (30)

Using the lens condition of Eq. (27) on the left-hand side of Eq. (A3) results in

$$\begin{aligned}&\int_{-\infty}^{\infty} \exp\left[-\frac{it''^2}{2\gamma} + \frac{i}{2\Phi_b}(t''-t_1)^2 + \frac{i(t''-t')^2}{2(\Phi_a-\Phi_c)}\right] dt'' \\ &= 2\pi\left|\frac{\Phi_b}{s}\right| \exp\left[\frac{i}{2\Phi_b}(t_1^2 - st'^2)\right] \delta\left(t' - \frac{t_1}{s}\right), \end{aligned} \tag{B1}$$

where s is defined in Eq. (29). Insertion of the previous formula into Eq. (A1) leads to Eq. (28).

[1] A. Gatti, E. Brambilla, and L. Lugiato, in *Progress in Optics*, Vol. 51, edited by E. Wolf (Elsevier, Amsterdam, 2008), p. 251.
[2] D. V. Strekalov, A. V. Sergienko, D. N. Klyshko, and Y. H. Shih, Phys. Rev. Lett. **74**, 3600 (1995).
[3] T. B. Pittman, Y. H. Shih, D. V. Strekalov, and A. V. Sergienko, Phys. Rev. A **52**, R3429 (1995).
[4] Y. H. Shih, Rep. Prog. Phys. **66**, 1009 (2003).
[5] R. S. Bennink, S. J. Bentley, and R. W. Boyd, Phys. Rev. Lett. **89**, 113601 (2002).
[6] A. Gatti, E. Brambilla, M. Bache, and L. A. Lugiato, Phys. Rev. A **70**, 013802 (2004).
[7] F. Ferri, D. Magatti, A. Gatti, M. Bache, E. Brambilla, and L. A. Lugiato, Phys. Rev. Lett. **94**, 183602 (2005).
[8] A. Gatti, M. Bache, D. Magatti, E. Brambilla, F. Ferri, and L. A. Lugiato, J. Mod. Opt. **53**, 739 (2006).
[9] M. Tsang and D. Psaltis, Phys. Rev. A **73**, 013822 (2006).
[10] V. Torres-Company, H. Lajunen, J. Lancis, and A. T. Friberg, Phys. Rev. A **77**, 043811 (2008).
[11] M. Bellini, F. Marin, S. Viciani, A. Zavatta, and F. T. Arecchi, Phys. Rev. Lett. **90**, 043602 (2003).
[12] S. Viciani, A. Zavatta, and M. Bellini, Phys. Rev. A **69**, 053801 (2004).
[13] I. A. Walmsley and C. Dorrer, Adv. Opt. Photon. **1**, 308 (2009).
[14] Y. Cai and S.-Y. Zhu, J. Opt. Soc. Am. A **22**, 1798 (2005).
[15] J. Liu, A. Tan, and Z. Hong, Opt. Commun. **282**, 3524 (2009).
[16] A. F. Abouraddy, B. E. A. Saleh, A. V. Sergienko, and M. C. Teich, J. Opt. Soc. Am. B **19**, 1174 (2002).
[17] H. M. Ozaktas, Z. Zalevsky, and M. A. Kutay, *The Fractional Fourier Transform with Applications in Optics and Signal Processing* (Wiley, Chichester, 2001).
[18] B. H. Kolner and M. Nazarathy, Opt. Lett. **14**, 630 (1989).
[19] V. Torres-Company, Ph.D. thesis, University of Valencia, 2008.
[20] B. H. Kolner, IEEE J. Quantum Electron. **30**, 1951 (1994).
[21] B. E. A. Saleh and M. C. Teich, *Fundamentals of Photonics*, 2nd ed. (Wiley, Hoboken, 2007).
[22] A. Valencia, M. V. Chekhova, A. Trifonov, and Y. Shih, Phys. Rev. Lett. **88**, 183601 (2002).
[23] F. Boitier, A. Gorard, E. Rosenthal, and C. Fabre, Nature (London) Phys. **5**, 267 (2009).
[24] L. Mandel and E. Wolf, *Optical Coherence and Quantum Optics* (Cambridge University Press, Cambridge, 1995).
[25] D.-Z. Cao, J. Xiong, S.-H. Zhang, L.-F. Lin, L. Gao, and K. Wang, Appl. Phys. Lett. **92**, 201102 (2008).
[26] K. W. C. Chan, M. N. O'Sullivan, and R. W. Boyd, Opt. Lett. **34**, 3343 (2009).
[27] B. I. Erkmen and J. H. Shapiro, Phys. Rev. A **79**, 023833 (2009).
[28] O. Katz, Y. Bromberg, and Y. Silberberg, Appl. Phys. Lett. **95**, 131110 (2009).
[29] F. Ferri, D. Magatti, L. A. Lugiato, and A. Gatti, Phys. Rev. Lett. **104**, 253603 (2010).
[30] A. W. Lohmann, J. Opt. Soc. Am. A **10**, 2181 (1993).
[31] T. Shirai, T. Setälä, and A. T. Friberg (in preparation).
[32] J. W. Goodman, *Introduction to Fourier Optics*, 3rd ed. (Roberts & Company, Englewood, 2005).
[33] Y. Cai and S.-Y. Zhu, Phys. Rev. E **71**, 056607 (2005).
[34] L. Basano and P. Ottonello, Am. J. Phys. **75**, 343 (2007).
[35] C. Dorrer and I. Wamsley, in *Phase-Space Optics*, edited by M. Testorf, B. Hennelly, and J. Ojeda-Castañeda (McGraw-Hill, New York, 2010), p. 337.